

Face2PPG: An unsupervised pipeline for blood volume pulse extraction from faces

Constantino Álvarez Casado^{1*} and Miguel Bordallo López^{1,2}

¹*Center for Machine Vision and Signal Analysis, University of Oulu, Finland.

²Cognitive technologies for intelligence, VTT Technical Research Centre of Finland Ltd, Oulu, Finland.

*Corresponding author(s). E-mail(s): constantino.lvarezcasado@oulu.fi;
Contributing authors: miguel.bordallo@oulu.fi;

Abstract

Photoplethysmography (PPG) signals have become a key technology in many fields such as medicine, well-being, or sports. Our work proposes a set of pipelines to extract remote PPG signals (rPPG) from the face, robustly, reliably, and in a configurable manner. We identify and evaluate the possible choices in the critical steps of unsupervised rPPG methodologies. We evaluate a state-of-the-art processing pipeline in six different datasets, incorporating important corrections in the methodology that ensure reproducible and fair comparisons. In addition, we extend the pipeline by proposing three novel ideas; 1) a new method to stabilize the detected face based on a rigid mesh normalization; 2) a new method to dynamically select the different regions in the face that provide the best raw signals, and 3) a new RGB to rPPG transformation method called Orthogonal Matrix Image Transformation (OMIT) based on QR decomposition, that increases robustness against compression artifacts. We show that all three changes introduce noticeable improvements in retrieving rPPG signals from faces, obtaining state-of-the-art results compared with unsupervised, non-learning-based methodologies, and in some databases, very close to supervised, learning-based methods. We perform a comparative study to quantify the contribution of each proposed idea. In addition, we depict a series of observations that could help in future implementations.

Keywords: Remote photoplethysmography (rPPG), Pulse rate estimation, Biosignals, Face Analysis

1 Introduction

Photoplethysmography (PPG) signals have become a key technology in many fields such as medicine, well-being, or sports. The technology utilizes a light source and a photodetector to measure the blood volume pulse (BVP) as light variations in skin tissues [1][2]. In medicine, PPG analysis is a basic and common tool in healthcare services to monitor vital signs such as heart rate

(HR) or oxygen saturation (SpO_2) [3]. In well-being, it became increasingly important thanks to the success of wearable devices that analyze sleep disorders [4], cardiovascular disorders [5], or detection of stress and meditation [6]. In sports, PPG analysis became an important tool to improve the intrinsic and extrinsic athletes' performance [7].

Remote PPG (rPPG) imaging is a contactless version of this technology that uses video

cameras, usually consumer-grade RGB or near-infrared cameras, and ambient light sources. It works by recording a subject's face or body parts with visible skin areas and analyzing the subtle color variations or motion changes in skin regions [8]. The remote PPG technique allows for non-invasive evaluation and monitoring of users in services, such as healthcare. Hence, the technology could offer significant advantages compared to contact-based devices if it becomes reliable [9].

Nowadays, there are two types of approaches to recover physiological signals from videos: unsupervised, non-learning-based methods that rely mostly on signal processing solutions, and learning-based or deep learning approaches [10].

Supervised, learning-based approaches mainly propose end-to-end solutions that try to recover the physiological signals or their parameters by learning the extraction process from a training set of videos. On the other hand, unsupervised approaches aim to recover physiological signals by applying computer vision and signal processing techniques without learning from any prior data, based on a series of pipelined steps. A standard pipeline followed by most of the unsupervised solutions is depicted in Figure 1.

Most of the unsupervised rPPG methods proposed in the literature focus on recovering PPG signals mostly from static faces, disregarding challenges under real scenarios in real world applications such as fast face and head movements, extreme light conditions, facial expressions, illumination changes, occlusion, or distance from the camera to the subject.

This article focuses on improving the performance of state-of-the-art rPPG unsupervised, non-learning-based methods with emphasis on all system components. We tackle the improvement of the process by proposing a set of changes across the whole pipeline that result in a noticeable global improvement, performing an extensive evaluation and a framework to recover physiological signals from faces.

1.1 Contributions

In this article, we depict different performance problems and challenges to reliably recover PPG signals from faces. We improve several components of the rPPG pipeline with novel ideas. The main

contributions to the pipeline can be summarized as follows:

- We provide a new method to stabilize the movement and facial expression based on a rigid mesh normalization, ensuring that the raw RGB signals are measured from the same facial location regardless of the pose and movement.
- We provide a new method based on statistical and fractal analysis to dynamically select only the facial regions that supply the best raw signals, discarding those with higher noise or prone to artifacts.
- We propose a novel rPPG method to transform the RGB signal into a PPG signal based on QR decomposition, named as Orthogonal Matrix Image Transformation (OMIT), which proves to be robust to video compression artifacts.

To prove the usefulness of our approach, we extensively evaluate a set of rPPG methods with four different pipelines across several datasets. Our experiments include modifications to the original evaluation pipeline to increase the fairness and reproducibility of the comparative results.

2 Related work

In the last few years, rPPG research has progressed from the filtering and simple processing of the variation of the facial skin color, to sophisticated multi-step processing pipelines and end-to-end supervised learning methods with dedicated architectures.

2.1 Unsupervised methods

Unsupervised or non-learning based methods focus on the recovery of physiological signals by applying computer vision and signal processing techniques as a system with several steps. These methods focus on obtaining the blood volume pulse (BVP) signal by finding skin areas suitable to extract the raw RGB signals, using face detection, tracking, and segmentation techniques. After that, these methods carefully process these raw RGB signals to separate the physiological signals contained in the subtle variations of the skin color from the rest of the information (motion, illumination changes, or facial expressions among others) by applying filtering and different ways of combining the RGB signals into a rPPG signal.

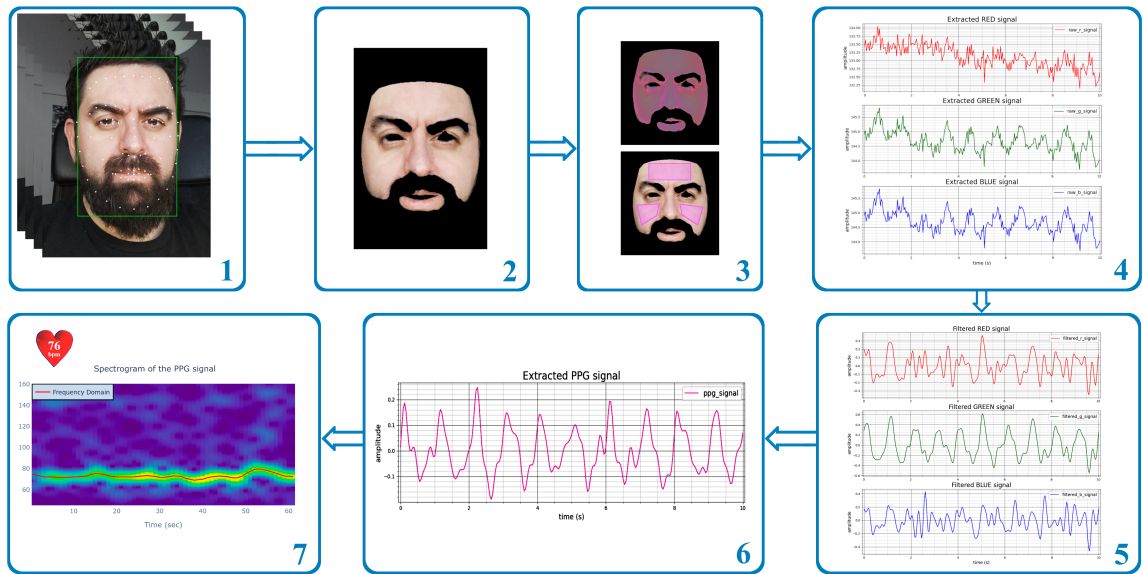


Fig. 1 Typical unsupervised based methodology for remote photoplethysmographic (PPG) imaging using a RGB camera. It comprises several steps: 1) Face detection and alignment 2) Skin segmentation 3) ROI selection 4) Extraction of the raw signals from ROIs 5) Filtered signals 6) RGB to PPG transformation 7) Spectral analysis and post-processing.

Most of the studies focus mainly on this transformation component using similar approaches and components for the rest of the process [11].

In 2008, Verkruysse et al. [12] proposed the first study on extracting remote PPG signals using an inexpensive consumer-grade RGB camera. The study showed how the green channel of the camera contains enough rich, significant information to recover signals such as the heart pulse. In 2010, Poh et al. [13] proposed the recovery of physiological signals by applying blind source separation (BSS) technique to remove the noise. Concretely, they used Independent Component Analysis (ICA) to uncover the independent source signals. Similar to this work, in 2011, Lewandoska et al. [14] proposed Principal Component Analysis (PCA) to reduce computational complexity in comparison to Independent Component Analysis with similar accuracy performance. In 2013, De Haan et al. [15] proposed a chrominance-based method (CHROM) to separate the specular reflection component from the diffuse reflection component which contains pulsatile physiological signals, both reflected from the skin and based on the dichromatic reflection model. In 2014, De Haan and van Leest [16] define a Blood-Volume Pulse (PBV) vector that contains the signature of the specific blood volume variations in the skin, removing noise and motion artifacts. In the

same year, Li et al. [17] focused on removing the human motions and artifacts from the RGB signals by applying Normalized Least Mean Square (NLMS) adaptive filter. They perform this rectification step by assuming both the face ROI and the background as Lambertian models that share the same light source. In 2016, Wang et al. [18] proposed a data-driven algorithm by creating a subspace of skin pixels and the computation of the temporal rotation angle of the computed subspace between subsequent frames to extract the heart rate pulse. In 2016, Yang et al. [19] proposed the CIELab color space (LAB) transformation as a more robust color space to extract pulse rate signals due to the high separation between the intensity and chromaticity components, less sensitive to human body movements. The study also demonstrates that the *a* channel has better signal-to-noise ratio (SNR) than the green channel in RGB color space. In 2017, Wang et al. [20] proposed a new plane-orthogonal-to-skin (POS) algorithm that finds pulsatile signals in an RGB normalized space orthogonal to the skin tone. In 2018, Pilz et al. [21] proposed the Local Group Invariance (LGI) method, a stochastic representation of the pulse signal based on a model that leverages the local invariance of the heart rate, as a quasi-periodical process dynamics, obtained by recursive inference to remove extrinsic factors such

as head motion and lightness variations. In 2020, Gudi et al. [22] proposed an unsupervised method with emphasis on motion suppression and novel filtering based the head-orientations (FaceRPPG).

In general, unsupervised methods try to recover the blood volume pulse signal as a photoplethysmography of the face. The main efforts have been made in finding suitable ways of transforming noisy RGB signals into reliable PPGs, while the impact of other components of the system such as face detection and tracking, have been mainly disregarded. Our contribution addresses the unsupervised rPPG process as a system with multiple components that can be improved separately.

The main advantage of unsupervised methods is that they do not require specific training data, and the results translate very well to different datasets and measurement setups, since they aim at measuring the blood volume pulse signal as it arrives to different regions of the face. However, since these methods do not include any learning component, their performance is very much affected by the different nature of this measured facial signal with respect to the reference signals considered the ground truth, which are mainly based on ECG signals or PPG signals obtained at a distant point (e.g. the head or the finger). Therefore, even for normal individuals that do not present anomalies, small differences in the resulting signals in terms of synchronicity and dynamic range are to be expected.

2.2 Supervised methods

Deep Neural Networks (DL) and especially *Convolutional Neural Networks* (CNN) approaches have gained attention and become popular tools in computer vision and signal processing tasks, including healthcare-related tasks. As of 2018, supervised or learning-based methods to compute HR or other vital signs started to arise increasingly in the literature. Among the most relevant learning-based remote PPG methods, in 2018, Špetlík et al. [23] proposed a two-step convolutional neural network to estimate a heart rate value from a sequence of facial images. HR-CNN is a trained end-to-end network composed by two components, an Extractor and a HR Estimator. The same year, Chen and

McDuff [24] proposed DeepPhys, another end-to-end solution based on a deep convolutional network that estimates HR and breathing rate (BR). The approach performs a motion analysis based on attention mechanisms and a skin reflection model using appearance information to extract the physiological signals. In 2019, Niu et al. [25] proposed RhythmNet, an end-to-end solution based on spatial-temporal mapping to represent the HR signals in videos. The approach also exploits temporal relationships of adjacent HR estimations to perform continuous heart rate measurements. The same year, Yu et al. [26] proposed a two-stage end-to-end solution. The first part of the network, named as STVEN, is a Spatio-Temporal Video Enhancement Network to improve the quality of highly compressed videos. The second part of the approach, named as rPPGNet, is the 3D-CNN network that recovers the rPPG signals from the enhanced videos. The authors claim that the proposed rPPGNet produces very rich rPPG signals with curve shapes and peak locations. In 2020, Yu et al. [27] further proposed other end-to-end approach for remote HR measurement based on Neural Architecture Search (NAS). AutoHR is comprised by three ideas: a first stage that discover the best topology network to extract the physiological signals based on Temporal Difference Convolution (TDC); a hybrid loss function based on temporal and frequency constrains; and spatio-temporal data augmentation strategies to improve the learning stage. The same year, Lee et al. [28] proposed a transductive meta-learner based on a LSTM estimator and Synthetic Gradient Generator that adjusts network weights in a self-supervised manner. In 2021, Song et al. [29] proposed a two-stage hybrid method called PulseGAN. The approach starts with the unsupervised extraction of noisy PPR signals using CHROM as a first stage. The second stage is a generative adversarial network (GAN) that generates realistic rPPG pulse signals from the recovered signals in the first stage.

Supervised rPPG methods, mostly based on deep learning, result in highly accurate setups since they mainly propose end-to-end solutions that try to recover the physiological signals or heart rate values from videos without intermediate steps [30], except maybe some basic preprocessing. These methods attempt to directly learn the reference contact-based PPG ground-truth signals

obtained from the finger by observing noisy patterns shown in the face. The result is a black box that recovers a physiological signal from video frames without a clear understanding of how it was achieved. We believe this limitation impacts directly on how these signals can be used further to train models that fulfill the standards and requirements of some critical applications, such as healthcare [31], or domains where the data available for training is scarce and anomalous signals are likely to be present.

3 Unsupervised blood volume pulse extraction methodology

In our work, we use a standard methodology in unsupervised rPPG approaches to extract the blood volume changes from facial videos and to derive important parameters from them. We follow a modular pipeline with several components, as depicted in Figure 1. The pipeline can roughly be split into three big blocks: the selection of measuring regions of the face, the extraction of rPPG biosignals from raw variations in color or texture, and the computation of the heart rate or other parameters using the extracted signals.

The pipeline comprises of 8 main modules sequentially connected:

1. **Database interface:** it includes the interfaces to read the data (videos, images and reference signals) of several publicly available databases.
2. **Face detection and alignment:** starting step that handles the detection and the alignment of the face at every frame. Face detection gives the coordinates where the face is located in the frame. Face alignment models detect several facial points in the detected face. It plays a critical role since these points are used to select regions of interest, patches or simply using them as segmentation coordinates.
3. **ROI selection:** step to select the regions of interest of the face based on a color skin segmentation or selection of patches based either on face location or the coordinates of the landmarks coordinates.
4. **RGB extraction:** extraction of the raw signal from a window of several RGB frames. The value at every sample is computed using the

mean value of the pixels contained in the mask or patches selected in the previous step.

5. **Pre-processing:** block mainly to filter the extracted raw RGB signal to adequate it to our band of interest. Filtering is a significant factor in properly recovering the BVP signal. Remote PPG signals usually present trends and noise in the frequency spectrum of the camera sample rate. The band of interest to recover the heart-related signal is between 0.75 and 4.0 Hz.
6. **RGB to PPG transformation (rPPG):** step where the RGB filtered signal is transformed to a PPG signal using a transformation method. Remote PPG methods are one of the core blocks in this topic since it is the component that transforms RGB signals into physiological signals. The main idea behind all the included methods is the combination of the RGB channels to convert them into a pulse signal.
7. **Frequency analysis:** spectrum analysis of the rPPG and reference ground-truth (BVP or ECG) signals to estimate the heart rate.
8. **Evaluation:** it includes an error and statistical analysis to compare the estimated heart rate from the rPPG and the estimated heart rate from the reference ground-truth signals.

3.1 Baseline pipeline

In our work, we start from an open-source framework for the evaluation of remote PPG methods, implemented in Python and called *pyVHR* (short for Python tool for Virtual Heart Rate)[32]. This framework includes an extensible interface to integrate several datasets, multiple methods and choices for each processing step, and extensive assessment and visualization tools. We use version 0.0.4 of the PyVHR framework, which we will refer to as *Baseline* pipeline onward.

4 Face2PPG pipelines

The *Baseline* pipeline presents a few shortcomings that might result in inaccurate or unfair assessments. We incrementally improve it by introducing several changes in multiple steps, and propose three new versions that we name *Improved*, *Normalized* and *Multi-region* pipelines.

These pipelines focus on the handling of the face in unconstrained conditions, since it is one of

the critical parts of the process to extract remote photoplethysmograms. It has to be noted that most of the unsupervised approaches have focused mainly on developing RGB to PPG conversion methods (sometimes called just rPPG methods), but they have not payed much attention to other steps of the pipeline. In this article, we emphasize the importance of every step when extracting and evaluating remote PPG signals from faces.

4.1 Improved pipeline

To mitigate its shortcomings, we modified the *Baseline* pipeline to incorporate a few minor changes that increase reproducibility and enable fairer comparison of different methods. We name this modified version as *Improved* pipeline. We enumerate and describe these changes as follows:

Face detection: The *Baseline* pipeline includes two well-known face detectors: one based on convolutional neural networks known as MTCNN [33] and a *Dlib* implementation based on HOG [34][35]. We use instead a new deep learning-based face detection method based on a Single Shot Multibox Detection network (SSD) [36], implemented in *OpenCV* library. This face detector outperforms the *Baseline* pipeline detectors in terms of accuracy, size of the models, and computational speed [37].

Face alignment: The *Baseline* pipeline includes two well-known face landmark detectors, the MTCNN detector [33] that computes 5 landmark points in the face (eyes, nose and mouth corners) and the *Dlib* implementation of the ERT method [38][35]. We use instead a deep learning approach named DAN (Deep Alignment Network) [39] which gives exceptional performance in terms of accuracy, even in challenging conditions [40] as shown in Figure 2. For a faster, real-time face alignment, we have added a more accurate, faster, and smoother model for the ERT *Dlib* face landmarks detector [40]. These models both infer 68 landmark points defined by the Multi-PIE landmark scheme [41].

Filtering: The *Baseline* pipeline only considers a pre-filtering scheme before the RGB to PPG transformation. The pipeline offers three types of filter: detrending (Scipy or Tarvainen methods), bandpass filtering (FIR filter with Hamming window and Butterworth IIR filter), and a Moving average filter (MA) that removes various base



Fig. 2 Facial landmark detection using DAN model under extreme head poses and frontal faces.

noises and motion artifacts of the signals. We have added the possibility of using Kaiser windows when applying FIR filtering. A Kaiser-Besel window maximizes the energy concentration in the main lobe, and it is highly recommended to filter biosignals [42]. In addition, we have introduced the possibility of applying also post-filtering, performed after the RGB to PPG conversion, since the literature suggests that some conversion methods perform better this way [43].

RGB to PPG transformation (rPPG):

The *Baseline* pipeline includes several reference methods such as POS [20], CHROM [15], GREEN[12], PCA[14], ICA[13], SSR [18], LGI [21] and PVB [16]. We have added one method based on selecting the chroma channel *a* after applying a CIE Lab color space transformation. CIE Lab separates the lightness information (channel L) from the chroma information (channels *a* and *b*). The chrominance components have a more significant dynamic range than the red, green, and blue channels in RGB color space [19]. In addition, it correlates with skin color and related parameters and describes better the subtle changes occurring in them [44].

Spectral analysis: In the original framework, the ground-truth pulse rate is estimated using Short Time Fourier Transform (STFT) when the ground-truth signal is a Blood Volume Pulse (BVP) signal, and R-Peak detection and RR interval analysis when the ground-truth signal is an ECG signal. In the *Baseline* pipeline, the recovered PPG signals are processed instead using the Welch's spectral density estimation. This mismatch introduces the possibility of unfair evaluation. We modified the pipeline so the ground-truth BVP signal and the rPPG signal are processed using the same spectral analysis algorithm and similar parameters such as the overlap or FFT length.

Evaluation: It can be expected that the reference BVP (PPG) signals taken in the finger

and the rPPG signals extracted from the face are not perfectly synchronized or show the same dynamic range. We show an example in the Figure 3. We can observe also a clear asynchrony in the heart rate estimation, as shown in Figure 4. These time shifts and morphological differences can be produced by several factors, both technical and physiological. Some of these effects are the distance between the optical sensors or the contact force effect of the finger PPG oximeter [45], different filtering parameters [46], individual variations among subjects [47], variability in the measurement site [48] and even blood perfusion differences in different body regions [49], among others. We mitigate some of the effects caused by comparing fundamentally different signals by adding a new parameter in the dataset interface that aligns both signals and both in time and dynamic range, resulting in a fairer estimation of the error between ground-truth HR estimation and rPPG HR estimation. The parameter has been adjusted for each dataset globally, using a mostly heuristic approach due to lack of detailed information of the measurement setups.

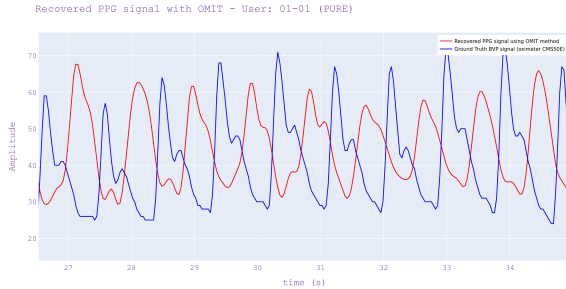


Fig. 3 Delay between the reference BVP signal and the remote PPG signal recovered using the proposed pipelines. This delay can be induced by several factors such filtering (since the GT BVP signal comes already filtered), blood perfusion differences or camera distance among others.

4.2 Normalized pipeline

Our *Normalized* pipeline introduces two significant changes compared to the previous ones, a segmentation approach based on geometric normalization, and a novel RGB to PPG transformation method, robust to compression artifacts.

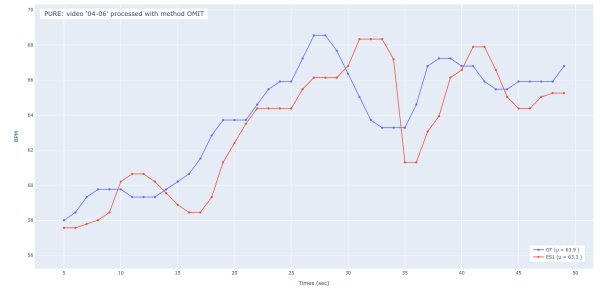


Fig. 4 Estimated HR from the reference BVP signal and the extracted facial rPPG signal using the *Baseline* pipeline. We can observe a clear asynchrony due to the different signal sources.

4.2.1 Geometric segmentation and normalization

One of the critical steps in the non-contact PPG extraction is the process related to skin segmentation, since it is the source to recover the desired physiological signals. Most of the unsupervised methods and pipelines rely on simple thresholding on different color spaces for skin color segmentation [32], from inefficient fixed RGB segmentation to adaptive HSV segmentation. These pixel-level techniques suffer from generalization due to the variability of skin tones, illumination changes, and complex backgrounds. It is not easy to define clear boundaries between the skin and non-skin pixels, especially due to the variability of the facial regions measured across different frames of a single video. Framewise skin segmentation based on neural networks (e.g., uNET) suffers similar problems, sometimes caused by the small number of annotated facial skin masks, resulting in underfitted models.

We propose to use instead a geometrical segmentation scheme that uses fiducial landmark points detected in the face. Although some inter-frame jittering due to the landmarks variability still remains and produces changes in the skin mask across the video frames, this is noticeably lower than using skin color segmentation. To perform this segmentation, we have extended the set of landmark points from 68 to 85 landmark points by interpolation, and created a fixed facial mesh composed of 131 triangles and fix their coordinates as a typical frontal face, as shown in Figure 5.

Our segmentation approach normalizes the face on each frame by mapping every triangle in the current detected face to the triangles in

the normalized shape as shown in Figure 5. This approach generates a spatiotemporal matrix of normalized faces that ensures that we measure the signals in the same facial regions consistently across frames, regardless of the pose and movement.



Fig. 5 Normalization of the face to fixed coordinates. From left to right, we observe the landmark points detected in the face, the face mesh with a fixed set of triangles and the normalized face after mapping each triangle to a fixed set of coordinates.

4.2.2 Orthogonal Matrix Image Transformation (OMIT)

To increase the robustness of the RGB to PPG transformation process in the presence of noise, we propose a new method that we name *Orthogonal Matrix Image Transformation* (OMIT). Based on matrix decomposition, it generates an orthogonal matrix with linearly uncorrelated components representing orthonormal components in the RGB color basis to recover the physiological signals. To do this, we use the QR factorization method [50] to find linear least-squares solutions in the RGB space using Householder Reflections [51]. We follow Equation 1:

$$A = Q * R \quad (1)$$

where $A \in R^{nxk}$ and is the input RGB matrix, $Q \in R^{nxk}$ is the orthonormal basis for $R(A)$, and $R \in R^{kxk}$ is an upper-right triangular and invertible matrix which shows what columns of Q are dependent.

OMIT has several advantages over other decomposition methods such as Principal Component Analysis (PCA) or Singular Value Decomposition (SVD), especially in terms of mathematical stability, computational efficiency, and robustness [52].

4.3 Multi-region pipeline

Extracting only one signal from the whole face or skin mask can result in a very noisy signal. However, the previously described segmentation skin produces a set of facial regions that can be analyzed separately. Due to partial occlusions, extreme head poses, illumination variations, or shades, among others, some of these regions might present very noisy signals with low dynamic ranges. Previous methods have proposed to select fixed patches in the face, where a priori, the blood perfusion should be more observable (e.g., forehead and cheeks). This approach works relatively well when the videos show quasi-static individuals in fixed environments, but fail when presented with fast movements or strong face rotations. To mitigate the impact of these challenges, we propose to modify the pipeline by introducing a dedicated block that automatically and dynamically selects those regions that contain the raw signals with higher quality. We name the resulting framework as *Multi-Region Pipeline*.

4.3.1 Dynamic multi-region selection

To dynamically select the best facial regions, we propose a novel Dynamic Multi-Region Selection (DRMS) method, an approach that extracts signals in a fixed set of facial regions, and statistically analyze their quality to select whether each one of them should contribute to the final rPPG signal or if it should be discarded.

The DRMS process starts just after obtaining a segmented and normalized face in the previous block of the pipeline, by dividing the normalized face in a matrix of $n \times n$ rectangles (regions of interest) that contains a spatiotemporal representation of the face as depicted in Figure 6. Each region in the grid represents a signal in a sequence of frames.

Next, the process continues the analysis by computing several statistical parameters on each candidate region as well as in the global face. These statistical parameters are computed using windows of t seconds, both in time and frequency domains. We extract the mean, standard deviation, variance, signal-to-noise ratio (SNR), Katz Fractal dimension (KFD), number of zero-crossings (Z_c), sample entropy, detrended fluctuation analysis (DFA) and the energy in terms of local power spectral density (PSD).

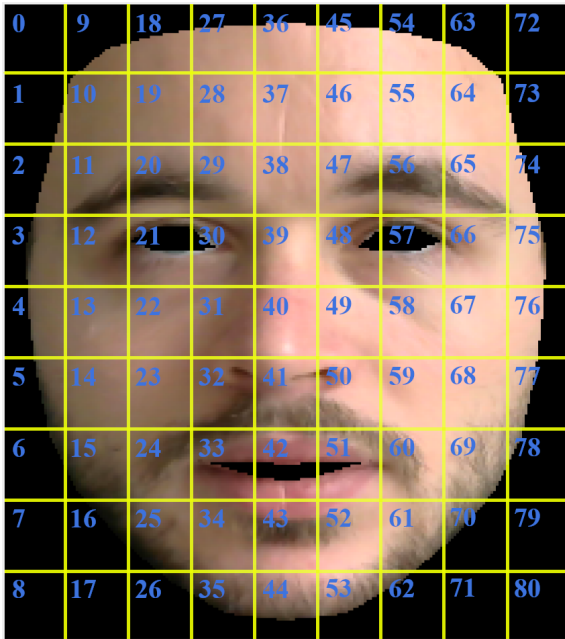


Fig. 6 Grid of candidate regions of interest over the normalized face. In this case, we have a grid comprised of 81 candidates (9x9) to extract the raw signals.

The dynamic selection is loosely based on fractal analysis, which portrays the scale of the randomness or how unpredictable a stochastic process is [53] [54]. It is based on standard deviation pruning, thresholding by the Katz fractal dimension, and the detrended fluctuation analysis (DFA) of each region. This analysis aims to identify one or more of the following fundamental time series features: self-similarity, power-law scaling relationship, and scale-invariance.

The first step is an initial pruning that removes those regions that do not contain any valuable information. We check the variance changes of every candidate rectangle along the time t and discard those that have zero variance (e.g. because they correspond to black rectangles).

Then, the regions are discarded based on the thresholding of the Katz's Fractal Dimension (KFD). KFD computes the fractal dimension (FD) of a signal based on the morphology, measuring the degree of irregularity and the sharpness of the waveform [55]. KFD gives an index D_{KFD} for characterizing the complexity of the signal. This value is computed as shown in the next equation:

$$D_{KFD} = \frac{\log_{10}(L/a)}{\log_{10}(d/a)} = \frac{\log_{10}(n)}{\log_{10}(d/L) + \log_{10}(n)} \quad (2)$$

where L is the total length of the PPG time series, a is the average of the Euclidean distances between the successive points of the sample, d is the Euclidean distance between the first point in the series and the point that provides the maximum distance with respect to the first point, and n is L/a . We discard every region with a relative D_{KFD} value below 0.85, as suggested in the literature.

The analysis continues by using Detrended Fluctuation Analysis (DFA), a statistical method widely used to detect intrinsic self-similarity in non-stationary time series, especially in fractal signals. DFA is a modified root mean square analysis of a random walk, designed to compute long and short-range non-uniform correlations in stochastic processes [56]. The method tells if each region rPPG signal shows the expected correlation with the signal from the global face signal, and if they are very noisy or contain artifacts of extrinsic trends [54]. The DFA exponent α is interpreted as an estimation of the Hurst parameter, and it is calculated as the slope of a straight line fit to the log-log graph from the fluctuation function. if $\alpha = 0.5$, the time series is uncorrelated. If $0.5 < \alpha < 1$ then there are positive correlations in the time series. If $\alpha < 0.5$ then the time series is anti-correlated. We discard those regions uncorrelated and negatively correlated.

After analyzing every region in the face in a sequence of frames (window of t seconds), we have a set of valid regions undergoing the last selection step, this time in terms of energy. We choose a fixed number x of regions with the highest energy, assuming that regions with high power spectral density will provide less noisy spectral responses. As the last step in the whole process, we aggregate the rPPG signals of the each one of the selected regions by summing them in the time domain. The resulting signal is then the final extracted rPPG that will be subsequently used to compute the heart rate in the spectral analysis step.

During the experiments, we have comparatively evaluated *Face2PPG* pipeline both in single-region mode (*Face2PPG-Single*) and in multi-region mode (*Face2PPG-Multi*).

5 Benchmark datasets and Evaluation Metrics

To evaluate the proposed methodology, we follow an extensive evaluation assessment as presented in the literature [32]. Our evaluation includes interfaces to work on six publicly available datasets:

PURE is a database that contains 10 subjects performing several controlled head motions [57]. The session was recorded using 6 different setups (steady, talking, slow translation, fast translation, slow rotation, and medium rotation), resulting in 60 sequences of 1 minute each. The videos were captured using an industrial-grade (*eco274CVGE* camera by *SVS-Vistek*) at a sampling rate of 30 Hz with an uncompressed cropped resolution of 640x480 pixels and an approximate average distance of 1.1 meters. The reference pulse data was captured in parallel using a contact-based FDA-approved fingertip pulse oximeter (*pulox CMS50E*) with a sampling rate of 60 Hz.

COHFACE is a remote photoplethysmography (rPPG) dataset that contains RGB videos with faces synchronized with heart rate and breathing rate of the recorded subjects [58]. It contains videos of 40 subjects (12 females and 28 males). The video sequences were recorded using a (*Logitech HD C525*) webcam at a sampling rate of 20 Hz and a resolution of 640x480 pixels. The database includes a total of 160 videos, of approximately 1 minute. Reference physiological data was recorded using medical-grade equipment.

LGI-PPGI-Face-Video-Database is a database that contains 25 subjects, but only 6 were released officially. The age of the participants, primarily Caucasian, is in the range of 25-42 years [21]. It was recorded using a *Logitech HD C270* webcam at a sampling rate of 25 Hz and a resolution of 640x480 pixels, in uncompressed format with auto-exposure. Reference physiological measurements were recorded at the same time using a contact-based FDA-approved fingertip pulse oximeter (*pulox CMS50E*) with a sampling rate of 60 Hz. The database contains subjects in four different scenarios: resting, rotation, talking in the street and gym. An image with the four scenarios is depicted in Figure 7.



Fig. 7 LGI-PPGI database [21] contains four different scenario recordings. From left to right: 1) Resting, 2) Rotation or Head Motions, 3) Talking and 4) Gym.

UBFC-RPPG Video dataset is a rPPG database comprised by two different datasets: UBFC1 or simple and UBFC2 or realistic [59]. UBFC1 contains 8 videos where the participants were asked to sit still in an office room under unconstrained conditions and natural light. UBFC2 contains 42 videos under constrained conditions. It induces changes in the blood volume pulse by asking participants to perform mathematical games. The database presents a wide variety of ethnicity with different facial skin tones as shown in the Figure 8. For some of our experiments we use a smaller subset of the UBFC2 dataset [32]¹



Fig. 8 UBFC-RPPG database [59] contains mostly two different scenarios. UBFC1 contains videos recorded in an office room under unconstrained conditions and natural light (from left to right the first two images). UBFC2 contains videos under controlled conditions but performing a stress task (from left to right, the last two images).

The database was recorded using a webcam (*Logitech C920 HD Pro*) at a sampling rate of 30 Hz and a resolution of 640x480 pixels in uncompressed 8-bit RGB format. The duration of each video is approximately two minutes long. The reference physiological data was synchronized and recorded at the same time using a contact-based FDA-approved fingertip pulse oximeter (*pulox CMS50E*) with a sampling rate of 60 Hz.

MAHNOb-HCI is a multimodal database captured mainly for emotion recognition [60]. The database contains 27 young healthy participants, 16 females and 11 males between 19 and 40 years old. The database was recorded with several cameras. The frontal camera was an *Allied Vision*

¹The UBFC2 subset is comprised by 26 videos (Numbers 1, 3, 10, 11, 12, 13, 14, 15, 16, 17, 18, 20, 22, 23, 24, 25, 26, 27, 30, 31, 32, 33, 34, 35, 36 and 37)

Stingray F-046C colour camera with a resolution of 780x540 pixels at 60 frames per second. The videos in MAHNOB-HCI database are highly compressed in H.264/MPEG-4, making them very challenging for the extraction of remote PPG signals. The reference signals were captured using an ECG sensor from the *Biosemi active II* system with active electrodes. The database includes 527 facial videos with corresponding physiological signals. For most of our experiments, we use a smaller subset of MAHNOB subset comprised by 36 videos [32].²

The evaluation of the datasets is done by comparing the estimations of the heart rates of both the extracted rPPG signal and the reference ECG or PPG signal. The evaluation includes both error and statistical analysis. We use three standard metrics that measure the discrepancy between our predicted heart rate $\hat{h}(t)$ and the reference heart rate $h(t)$. The standard metrics used to compute it are Mean Absolute Error (MAE), Root-Mean-Square Error (RMSE), and Pearson Correlation Coefficient (PCC) of the heart-rate envelope.

5.1 Reference data, ground-truth and evaluation protocol

The most common source of blood volume pulse (BVP) reference data in the datasets is PPG data from contact-based pulse oximeters. In most of the cases, these data is already filtered and does not require further preprocessing. In order to extract heart rate or other HRV parameters, the reference signals are processed using spectral analysis.

In the evaluation, we compute the error by comparing the heart rate and HRV parameters extracted from the reference (ground-truth) signals and the recovered PPG signal. Although direct comparison of signals (e.g. morphology) would be also possible, the fundamental differences between the extracted rPPG and the reference signals in terms of delay and scale due to different body measurement points and diverse collection devices make this comparison not very meaningful.

²The MAHNOB subset is composed by 36 videos (Numbers 10, 1198, 1576, 2094, 2226, 2604, 2634, 2888, 3388, 3644, 556, 808, 1042, 1322, 1590, 2114, 2246, 2606, 274, 3006, 3396, 3662, 800, 814, 1184, 152, 1698, 2120, 2346, 2624, 276, 3136, 34, 408, 806 and 926)

We have observed that the reference data offered in the datasets is not completely free of problems. For example, Figure 9, shows an example reference signal with a gap of approximately 2 seconds. These issues, caused by small deficiencies in data collection can lead to unfair disagreements in terms of error, especially for unsupervised methods.

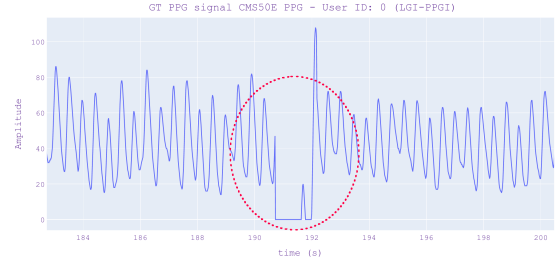


Fig. 9 Section of a reference PPG signal recorded with a fingertip contact-based pulse oximeter where we can observe an error of ≈ 2 seconds, probably due to movement of the finger and consequent lost of the signal tracking.

6 Experimental results

We evaluate and analyse the proposed methodologies and pipelines to extract remote photoplethysmography signals from all the benchmark databases. We compare the results across different improved processing pipelines and compare them with the state of the art for both supervised and unsupervised methods. The experiments are performed using a computer that includes an AMD® Ryzen(TM) 3700X 8-core processor at 3.6GHz.

6.1 Hyperparameters and configuration

Our framework is based on separate configuration files, in a similar manner as other frameworks [32]. These files contain the parameters that govern the pipeline and its components. In our experiments, we set the values for each pipeline component as follows:

Face detection uses a DNN OpenCV face detector with the default Tensorflow model.

Face alignment uses the DAN algorithm with one of the default models provided by the authors (*DAN-Menpo.npz*) [39]. Real-time configurations can use a modified ERT model [40].

DRMS uses a grid matrix of $n = 9 \times 9$. For D_{KFD}, we have selected the signals with a threshold of more than 0.85, and for DFA we set an α threshold between 0.75 and 1.0. We set the maximum number valid of regions as 32.

Filtering is performed using FIR filters with Kaiser windows, with the parameter $\beta = 25$. The filters use a bandpasss configuration between 0.75 and 4 Hz (corresponding to 45-240 bpm).

Signal Windowing uses sliding windows of 10 seconds and 1 second steps (9 seconds overlap).

6.2 Quantitative results

We provide an extensive evaluation of our three proposed pipelines and compare them with those of the baseline [32] with the standard configuration. We obtain results in six datasets. All datasets are comprised by videos with VGA resolution, but in two of them are heavily compressed (MAHNOB and COHFACE).

We measure the performance by computing the average of the MAE, the standard deviation of the MAE, and the median of the Pearson Correlation Coefficient of the envelope of the heart-rate. We evaluate the pipelines using ten rPPG methods (RGB to PPG signal conversion methods), including our proposed OMIT conversion. The results detail the impact of the improvements in each pipeline and are shown in Table 1.

We can observe how the Multi-region pipeline, integrating all our proposed improvements, shows the best results across all six datasets. The results show improvements both in terms of MAE, the standard deviation of the error and the Pearson Correlation Coefficient of the heart-rate envelope.

When analyzing different RGB to PPG conversion methods (rPPG) it is difficult to make conclusions on which method is the best, since the results vary across different datasets. In any case, it can be seen that both CHROM and POS methods still show the best results in uncompressed databases across all pipelines, although closely followed by our OMIT proposed conversion. However, OMIT shows to work extremely well across highly compressed pipelines, obtaining the best results in the challenging MAHNOB dataset. In addition, we observe that some methods work better in some of the databases with different pipelines.

When comparing results across datasets, we can see that the mean average error fluctuates in a big range depending on the nature of the data. Datasets with good quality videos with static people, such as UBFC or PURE show an error well below 2 bpm, with relatively minor differences across videos, as reflected by the low standard deviation of the error. For the dataset containing natural movement in front of the camera, the LGI-PPGI dataset, the average error in the best case reaches almost 4 bpm, with a reasonable, but still high standard deviation across videos. The worst results correspond to those datasets with lower resolutions, MAHNOB and COHFACE, where the average error is between 8 and 12 bpm for best of the cases. This is expected since heavy video compresion and low illumination can lead to low Signal-to-Noise Ratio (SNR) and the loss of subtle variations of the signal [61][62].

In each dataset, the error presents variations along the different videos. This is shown in the standard deviation of the MAE, which reflects this variations. As a more detailed example, we computed the error and the Pearson Correlation Coefficient with its mean, maximum, minimum, and standard deviation for 10 RGB to PPG conversion methods, for the COHFACE and UBFC1 datasets and the Multi-region pipeline. We depict it graphically in Figure 10. It can be seen that for the high video quality dataset, there is some variability across rPPG conversion methods, while the variability among videos is relatively low. For the heavily compressed dataset, the error and its variability across videos is generally higher, but stable across different rPPG methods.

Although some variations across methods, dataset and pipelines exist, it is possible to conclude that the modification introduced in the pipelines shows a consistent improvement. Figure 11 shows the error reduction across the four pipelines, depicted as the best result for each database. Although the improvements are mostly consistent across datasets, those databases with faces mostly still in front of the camera (PURE and UBFC), show only modest improvements when compared with those achieved in complicated datasets with fast movements or heavily compressed videos (LGI-PPGI, COHFACE, MAHNOB), where the improvement is more noticeable.

Table 1 Error comparison between the baseline pipeline and our three proposed improved pipelines.

Pipeline	PPG Method	Databases											
		LGI-PPGI		COHFACE		MAHNOB		PURE		UBFC1		UBFC2	
		MAE \pm SD	PCC	MAE \pm SD	PCC	MAE \pm SD	PCC	MAE \pm SD	PCC	MAE \pm SD	PCC	MAE \pm SD	PCC
Baseline (+ PPG Method)	GREEN (2008) [12]	16.3 \pm 11.4	0.23	12.3 \pm 7.2	0.05	15.3 \pm 7.5	0.01	5.8 \pm 12.9	0.64	15.9 \pm 10.4	-0.04	8.1 \pm 11.7	0.60
	ICA (2010) [13]	11.2 \pm 11.4	0.22	11.1 \pm 5.8	0.20	14.9 \pm 6.2	0.17	4.4 \pm 5.2	0.36	5.8 \pm 6.0	0.44	10.4 \pm 7.2	0.41
	PCA (2011) [14]	10.9 \pm 12.1	0.22	10.4 \pm 5.7	0.27	11.0 \pm 5.4	0.17	1.9 \pm 1.7	0.77	4.5 \pm 1.8	0.43	5.2 \pm 3.9	0.58
	CHROM (2013) [15]	11.1 \pm 14.2	0.39	12.4 \pm 7.0	0.03	18.6 \pm 9.0	0.06	1.6 \pm 2.0	0.83	2.2 \pm 0.8	0.71	3.1 \pm 2.5	0.79
	PBV (2014) [16]	17.4 \pm 13.1	0.03	13.2 \pm 6.5	0.05	18.6 \pm 6.5	-0.02	3.6 \pm 3.7	0.45	8.9 \pm 6.0	0.30	5.5 \pm 7.0	0.63
	2SR (2016) [18]	10.1 \pm 8.9	0.31	11.8 \pm 7.5	0.02	17.5 \pm 5.3	0.05	3.7 \pm 7.1	0.73	4.1 \pm 3.8	0.64	5.7 \pm 5.6	0.40
	LAB (2016) [18]	10.9 \pm 10.8	0.35	11.2 \pm 5.6	0.03	20.5 \pm 10.3	0.05	2.4 \pm 3.5	0.64	7.5 \pm 7.8	0.39	12.5 \pm 13.2	0.39
	POS (2017) [20]	11.8 \pm 14.4	0.38	11.9 \pm 7.1	0.05	19.4 \pm 5.5	0.02	1.9 \pm 3.1	0.85	1.8 \pm 0.4	0.87	1.9 \pm 1.4	0.91
Improved (+ PPG Method)	LGI (2018) [21]	10.3 \pm 13.2	0.42	12.6 \pm 7.1	-0.01	19.0 \pm 5.5	0.05	3.2 \pm 3.5	0.59	2.4 \pm 1.0	0.70	8.7 \pm 6.3	0.40
	OMIT (2021)	9.5 \pm 11.1	0.48	12.4 \pm 6.6	0.04	19.9 \pm 9.0	0.13	2.3 \pm 4.9	0.65	5.9 \pm 7.1	0.89	5.8 \pm 8.2	0.82
	GREEN (2008) [12]	9.3 \pm 7.9	0.27	9.6 \pm 5.7	0.01	12.2 \pm 5.8	0.16	4.8 \pm 8.5	0.65	8.7 \pm 10.2	0.68	5.4 \pm 5.9	0.81
	ICA (2010) [13]	7.7 \pm 9.3	0.30	8.8 \pm 4.8	0.07	17.0 \pm 7.0	0.06	1.9 \pm 3.9	0.86	6.3 \pm 8.2	0.77	6.6 \pm 8.0	0.66
	PCA (2011) [14]	7.8 \pm 9.9	0.35	8.6 \pm 4.8	0.04	17.2 \pm 8.9	0.10	1.9 \pm 4.3	0.86	5.5 \pm 6.5	0.59	5.0 \pm 6.7	0.95
	CHROM (2013) [15]	4.8 \pm 5.6	0.46	8.3 \pm 4.4	0.03	14.4 \pm 7.1	-0.02	1.8 \pm 1.9	0.83	2.6 \pm 2.7	0.88	5.3 \pm 7.6	0.94
	PBV (2014) [16]	12.5 \pm 9.6	0.09	9.1 \pm 5.8	0.10	15.8 \pm 7.2	0.08	3.6 \pm 8.0	0.83	7.0 \pm 7.9	0.65	9.4 \pm 9.3	0.41
	2SR (2016) [18]	7.5 \pm 11.9	0.31	8.8 \pm 6.4	0.03	12.9 \pm 7.0	0.10	3.5 \pm 7.8	0.85	3.6 \pm 3.8	0.83	8.6 \pm 9.8	0.75
Normalized (+ PPG Method)	LAB (2016) [18]	6.0 \pm 6.6	0.37	8.5 \pm 4.6	-0.03	16.2 \pm 8.3	-0.01	2.6 \pm 6.5	0.87	3.0 \pm 2.6	0.73	7.5 \pm 8.8	0.39
	POS (2017) [20]	5.1 \pm 6.2	0.58	7.8 \pm 4.6	0.04	14.8 \pm 7.3	0.04	2.2 \pm 9.1	0.91	2.8 \pm 2.7	0.89	3.7 \pm 7.6	0.96
	LGI (2018) [21]	4.7 \pm 5.7	0.44	8.5 \pm 3.8	0.02	14.2 \pm 7.2	-0.09	4.2 \pm 8.2	0.78	3.0 \pm 2.4	0.72	4.8 \pm 7.0	0.90
	OMIT (2021)	4.4 \pm 5.7	0.53	7.5 \pm 3.9	0.03	15.3 \pm 5.9	-0.16	2.3 \pm 9.1	0.88	3.3 \pm 4.0	0.93	4.3 \pm 6.1	0.95
	GREEN (2008) [12]	13.2 \pm 9.7	0.23	13.1 \pm 7.5	-0.03	18.7 \pm 9.5	-0.16	12.4 \pm 13.5	0.22	7.5 \pm 4.4	0.46	9.0 \pm 8.6	0.29
	ICA (2010) [13]	10.9 \pm 9.2	0.33	12.3 \pm 5.1	-0.01	19.5 \pm 6.2	0.12	3.5 \pm 5.7	0.73	2.1 \pm 0.5	0.66	3.2 \pm 5.8	0.94
	PCA (2011) [14]	11.9 \pm 9.5	0.28	11.4 \pm 5.1	0.02	19.4 \pm 7.3	0.06	2.9 \pm 2.9	0.53	2.6 \pm 1.4	0.65	2.8 \pm 2.9	0.90
	CHROM (2013) [15]	6.9 \pm 5.8	0.47	9.5 \pm 4.3	-0.03	17.7 \pm 9.3	-0.06	1.7 \pm 2.1	0.78	1.5 \pm 0.5	0.88	2.0 \pm 2.8	0.95
Multi-region (+ PPG Method)	PBV (2014) [16]	11.1 \pm 8.3	0.11	12.1 \pm 5.9	0.01	18.3 \pm 10.1	0.03	10.3 \pm 12.4	0.37	1.7 \pm 0.7	0.88	4.3 \pm 4.4	0.85
	2SR (2016) [18]	12.0 \pm 9.6	0.26	9.1 \pm 4.6	0.03	15.2 \pm 7.9	-0.03	1.3 \pm 1.7	0.87	1.7 \pm 0.6	0.95	1.7 \pm 1.2	0.93
	LAB (2016) [18]	8.0 \pm 6.9	0.44	10.1 \pm 4.7	-0.03	17.8 \pm 11.3	-0.01	5.9 \pm 7.5	0.49	1.9 \pm 1.4	0.79	5.3 \pm 5.7	0.62
	POS (2017) [20]	8.7 \pm 8.4	0.50	9.4 \pm 4.8	0.10	18.1 \pm 9.1	-0.07	1.5 \pm 2.7	0.85	1.2 \pm 0.4	0.94	1.4 \pm 1.5	0.95
	LGI (2018) [21]	8.8 \pm 7.3	0.42	9.2 \pm 4.3	-0.01	15.2 \pm 7.0	0.01	2.6 \pm 3.5	0.63	1.8 \pm 0.6	0.76	3.6 \pm 5.3	0.85
	OMIT (2021)	9.0 \pm 8.0	0.39	10.6 \pm 5.2	-0.06	14.2 \pm 6.3	-0.08	2.2 \pm 3.2	0.80	1.4 \pm 0.5	0.91	3.4 \pm 5.3	0.87
	GREEN (2008) [12]	8.3 \pm 7.3	0.26	9.1 \pm 6.1	0.05	12.9 \pm 11.0	0.21	5.4 \pm 8.8	0.47	3.8 \pm 2.4	0.59	1.4 \pm 1.7	0.94
	ICA (2010) [13]	9.2 \pm 8.1	0.16	8.6 \pm 4.3	0.03	14.3 \pm 8.3	0.09	2.4 \pm 2.6	0.71	1.5 \pm 0.6	0.90	3.2 \pm 3.3	0.75
Baseline (+ PPG Method)	PCA (2011) [14]	9.5 \pm 9.7	0.22	8.6 \pm 4.0	0.04	16.3 \pm 8.1	0.17	2.4 \pm 3.1	0.72	2.0 \pm 1.0	0.75	3.5 \pm 4.0	0.67
	CHROM (2013) [15]	3.9 \pm 3.6	0.58	8.8 \pm 4.5	0.03	12.6 \pm 6.2	0.10	1.2 \pm 0.9	0.84	0.8 \pm 0.5	0.98	1.5 \pm 1.5	0.95
	PBV (2014) [16]	9.5 \pm 7.6	0.24	9.5 \pm 4.6	0.09	15.9 \pm 7.7	0.06	4.9 \pm 7.4	0.53	3.7 \pm 2.9	0.58	4.7 \pm 5.2	0.65
	2SR (2016) [18]	14.8 \pm 8.6	0.08	9.1 \pm 4.5	0.09	18.0 \pm 8.7	0.06	5.7 \pm 7.7	0.49	1.3 \pm 0.5	0.91	6.6 \pm 7.7	0.46
	LAB (2016) [18]	6.4 \pm 5.9	0.35	9.5 \pm 4.4	-0.03	14.6 \pm 7.1	0.03	3.0 \pm 4.6	0.68	1.0 \pm 0.5	0.96	2.5 \pm 2.4	0.81
	POS (2017) [20]	4.5 \pm 3.3	0.57	8.0 \pm 4.4	0.06	13.6 \pm 6.7	0.05	1.4 \pm 1.6	0.86	0.9 \pm 0.4	0.96	0.9 \pm 0.9	0.98
	LGI (2018) [21]	4.5 \pm 3.1	0.56	7.5 \pm 3.5	0.11	10.8 \pm 6.0	0.07	1.7 \pm 1.9	0.72	1.4 \pm 0.9	0.92	1.5 \pm 1.6	0.96
	OMIT (2021)	4.4 \pm 3.1	0.62	8.0 \pm 4.1	0.08	9.3 \pm 4.1	0.08	1.7 \pm 2.6	0.86	0.8 \pm 0.4	0.97	1.1 \pm 1.2	0.98

The results for MAHNOB and UBFC2 are computed in a smaller subset of videos, according to [32]. For LGI-PPGI, COHFACE, UBFC1 and PURE we use the full set of videos.

In this context, we argue that the proposed multi-region pipeline shows better performance when presented with videos collected in a more natural environment, especially when they show varied facial expressions, head movements, or illumination changes. To illustrate this, we disaggregate the results obtained on the LGI-PPGI dataset. This dataset is divided in four different scenarios. The resting scenario is a reference scenario where the participants are still in front of the camera with no head or facial movements and illumination, mostly static. In the rotation scenario, the subjects are also in the same setup, but the subjects perform a series of head motions and rotations. In the talking scenario, the subjects are in the wild (mainly in the street), under

unconstrained conditions talking in video conference mode with sudden face and head motions. The illumination is natural light with strong backlight conditions in some of the videos, provoking low dynamic range (LDR) images. The last session represents a sports scenario recorded in a gym, where the subjects freely perform a physical exercise on a static bicycle. The illumination is mainly ceiling lights. In some of the videos, we can appreciate the flickering effect due to the ceiling lights. These last two could represent typical scenarios where we would need to remotely extract physiological signals, such as during video conferences for remote healthcare or sport performance monitoring. We show the results in Table 2. We compare the baseline and multiregion pipelines

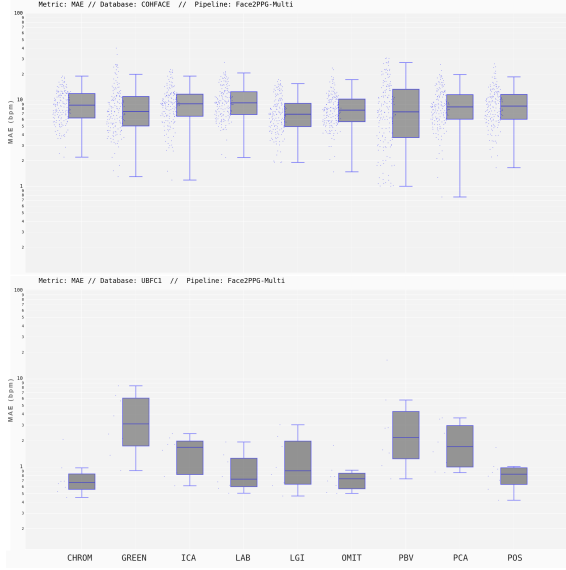


Fig. 10 MAE in logarithmic scale for COHFACE (up) and UBFC1 (down) databases using the Multi-region pipeline with 9 different rPPG methods. The middle line in the boxes indicates the median at every method.

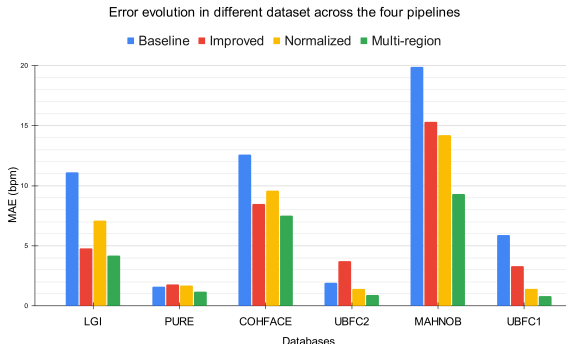


Fig. 11 Error evolution (best result) across the four pipelines in six benchmark datasets

using our proposed OMIT method for RGB to PPG conversion.

Table 2 Performance of the Baseline and Multi-region pipelines across LGI-PPGI dataset for different human activities. Examples of these scenarios are shown in Figure 7.

Scenario	Baseline			Multi-region		
	MAE \pm SD	PCC	RMSE	MAE \pm SD	PCC	RMSE
Resting	1.8 \pm 1.9	0.83	2.8	1.3 \pm 1.3	0.87	1.7
Rotation	5.2 \pm 3.2	0.10	9.4	5.1 \pm 2.8	0.58	7.6
Talking	9.5 \pm 9.8	0.59	11.3	5.8 \pm 3.9	0.57	7.5
Gym	23.2 \pm 11.4	0.16	27.6	7.5 \pm 4.8	0.76	11.1

The table shows that the Baseline and the Multi-region pipelines yield comparable results, both in terms of error and correlation with the ground truth, when they are evaluated in simple videos, such as *Resting* and *Rotation* scenarios. However, in challenging videos, such as the *Talking* scenario, the error is reduced almost to half, while in *Gym* scenarios the error is reduced three-fold. The Pearson Correlation Coefficient shows a similar trend, but it can be best appreciated in the *Gym* scenario.

6.3 Comparison with the state of the art

To illustrate the usefulness of our method, we compare our proposed pipeline with other supervised and unsupervised methods as presented in the state of the art. We compare the results in terms of both MAE and RMSE and show them in Table 3.

It can be seen that our method, relying on the multi-region pipeline obtains better results than all unsupervised methods, across all six benchmark datasets. Our results are also comparable to some recent supervised methods that require training on videos taken in similar conditions.

6.4 Qualitative results

In addition to quantitative experiments, we graphically show some examples of the obtained heart-rates for different pipelines and methods. Figure 12, shows the difference among four rPPG methods on the Multi-region pipeline, on a single video from the high resolution, PURE dataset, containing mostly static videos. We can observe that CHROM, OMIT and POS have similar performance when computing the heart rate evolution. On the other hand, the GREEN method, which is the worst in general, is incapable of tracking pulse rate in some sections of the measurement. The similarity between the estimated envelope (in red) and the ground-truth envelope (in blue), is reflected by the PCC metric.

Figure 13, shows the difference among four rPPG methods using the Multi-region pipeline in a video from MAHNOB database. Even when the person in the video is also static, the high compression of the video provokes a loss of detail and subtle variations in the raw RGB signals. However,

Table 3 Comparison of our proposed unsupervised method (best result) with state of the art supervised (orange) and unsupervised (blue) methods. Results with (*) are not directly comparable.

		Databases					
Metric	Method	LGI-PPGI	COHFACE	MAHNOB (*)	PURE	UBFC1	UBFC2 (*)
MAE (bpm \pm SD)	Face2PPG (Ours)	4.5 \pm 3.3	7.5 \pm 3.5	9.7 \pm 5.4	1.2 \pm 0.9	0.8 \pm 0.4	2.0 \pm 0.9
	CHROM (2013) [15]	9.4 \pm 12.6	12.4 \pm 7.0	18.6 \pm 9.0	1.6 \pm 2.0	2.2 \pm 0.8	8.3 \pm 10.9
	Li et al. (2014) [17]	-	19.9 \pm n/a	7.4 \pm n/a ¹	28.2 \pm n/a	-	-
	POS (2017) [20]	9.7 \pm 11.9	11.9 \pm 7.1	19.4 \pm 5.5	1.9 \pm 3.1	1.8 \pm 0.4	7.9 \pm 10.4
	FaceRPPG (2020) [22]	-	14.2 \pm 11.6	18.6 \pm 13.5	0.4 \pm 0.4 ²	-	2.7 \pm 6.7 ²
	HR-CNN (2018) [23]	-	8.1 \pm n/a	7.3 \pm n/a	1.8 \pm n/a	-	-
	DeepPhys (2018) [24]	-	-	4.6 \pm n/a	0.8 \pm n/a	-	-
	rPPGNet (2019) [26]	-	-	5.5 \pm n/a	-	-	-
	Meta-rPPG (2020) [28]	-	9.3 \pm 11.5	3.0 \pm 4.9	-	-	6.0 \pm 7.1
RMSE (bpm \pm SD)	Face2PPG (Ours)	6.7 \pm 5.1	9.8 \pm 4.6	12.5 \pm 5.8	1.8 \pm 1.9	1.1 \pm 0.5	2.8 \pm 3.0
	CHROM (2013) [15] [32]	11.4 \pm 13.7	16.4 \pm 7.9	22.1 \pm 8.7	3.0 \pm 4.8	4.8 \pm 3.4	10.3 \pm 13.5
	Li et al. (2014) [17]	-	25.6 \pm n/a	7.6 \pm 6.9 ¹	31.0 \pm n/a	-	-
	POS (2017) [20]	11.9 \pm 13.0	16.1 \pm 8.1	27.7 \pm 6.2	3.6 \pm 6.3	2.6 \pm 0.9	9.9 \pm 11.7
	FaceRPPG (2020) [22]	-	-	-	-	-	-
	HR-CNN (2018) [23]	-	10.8 \pm n/a	9.2 \pm n/a	2.4 \pm n/a	-	-
	DeepPhys (2018) [24]	-	-	-	1.5 \pm n/a	-	-
	rPPGNet (2019) [26]	-	-	7.8 \pm 7.8	-	-	-
	Meta-rPPG (2020) [28]	-	12.3 \pm n/a	3.7 \pm n/a	-	-	7.4 \pm n/a
	AutoHR (2020) [27]	-	-	5.1 \pm 4.3	-	-	-

(*) For this comparison, we use the full set of each database, including MAHNOB (527 videos) and UBFC2 (42 videos). ¹ The results by Li et al. [17] were obtained in a smaller subset of MAHNOB, using an adaptive filter that interpolated the heart-rate values when the quality of the rPPG signal was low. We reproduced the experiments with a fair configuration, obtaining a MAE of 15.5. ² The results of Gudi et al. [22] use an adaptive post-processing filtering of the HR values and were calculated in 15 second windows. According to their manuscript, the MAE expected when extrapolating to 10s is about 1.2 for PURE database and 4.1 for UBFC2.



Fig. 12 Comparison of the HR estimation with 4 different rPPG methods using the Multi-region pipeline. We show the estimated heart rate (red) extracted from the face, and from the contact-based reference PPG signal (blue), computed on a single video of the PURE dataset.

we can observe how methods such as CHROM or OMIT can tackle the problem of compression better than others such as GREEN or POS.

6.5 Evaluation of the number of regions

To evaluate the impact of the DMRS module in the Multi-region pipeline, we have designed

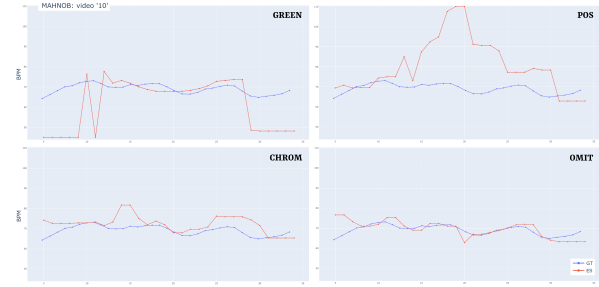


Fig. 13 Comparison of the HR estimation with 4 different rPPG methods using the Multi-region pipeline. We show the estimated heart rate (red) extracted from the face, and and from contact-based reference PPG signal (blue), computed on a single video of the MAHNOB dataset.

a complementary experiment that measures how the results are affected depending on the number of facial regions used in the initial grid. We use CHROM as the RGB to rPPG conversion method, while all parameters remain the same except the number of initial available regions to select. In addition to region grids, we also include in the comparison typical fixed regions of the face, such as the forehead and cheeks, depicted in 14.

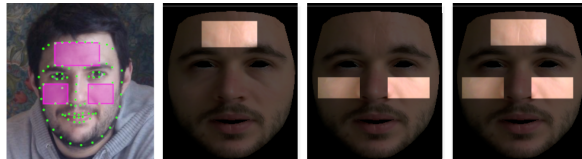


Fig. 14 Region selection based on normalized fixed patches. From left to right: face landmark detection, forehead patch, cheek patches and both combined.

For this experiment, the results are depicted in Table 4. They show how generally, a moderately large number of regions results in smaller errors. The approach using fixed patches shows comparable results to configurations with low number of regions and prove to be still useful in some cases.

Table 4 Impact of the number of regions in rPPG extraction using *Face2PPG-Multi* pipeline and CHROM.

Regions	LGI-PPGI			COHFACE		
	MAE \pm SD	PCC	RMSE	MAE \pm SD	PCC	RMSE
6 x 6	4.3 \pm 4.3	0.60	5.9	8.9 \pm 4.6	-0.03	11.0
7 x 7	4.1 \pm 3.5	0.62	5.6	8.9 \pm 4.4	0.01	11.0
8 x 8	4.0 \pm 3.4	0.64	5.7	9.0 \pm 4.3	0.03	11.1
9 x 9	3.9 \pm 3.6	0.59	5.5	8.8 \pm 4.5	0.03	11.0
10 x 10	4.0 \pm 3.4	0.63	5.7	9.2 \pm 4.4	-0.01	11.3
11 x 11	4.2 \pm 4.0	0.61	5.8	9.3 \pm 4.5	0.02	11.5
Forehead	5.4 \pm 6.3	0.63	7.5	11.6 \pm 5.5	-0.01	14.3
Cheeks	6.5 \pm 5.5	0.42	8.7	10.9 \pm 4.0	0.05	13.4
Combined	5.1 \pm 4.5	0.60	7.3	10.1 \pm 4.5	-0.01	12.6

7 Conclusion

In this article, we proposed a new unsupervised pipeline for the extraction of blood volume pulse (rPPG) signals from facial videos. To enable a fair comparative evaluation among methods, we solved a set of smaller technical challenges such as problems with signal synchronization, use of different spectral analysis methods in extracted and reference signals, or inconsistent use of pipeline modules such as face detection and tracking or filtering. We proposed three novel contributions that improve the extraction of rPPG signals, especially in challenging conditions. First, we included a face normalization module, based on facial landmarks and a fixed triangle mesh that allowed the extraction of signals at exactly the same facial regions in a consistent manner. Second, we added the dynamic selection of facial regions that allowed to statistically discard those regions showing noise

and artifacts. Finally, we proposed a novel RGB to PPG conversion method that increased the robustness of the extraction against compression artifacts. Our enhanced pipeline works in a purely unsupervised manner, and it is directly applicable in datasets collected in multiple conditions without any need of training data. The proposed pipeline achieves state-of the-art results across multiple databases when compared with other unsupervised methods and shows comparable results to other unsupervised methods.

References

- [1] Elgendi, M.: On the analysis of fingertip photoplethysmogram signals. *Current cardiology reviews* **8**, 14–25 (2012). <https://doi.org/10.2174/157340312801215782>
- [2] Allen, J.: Photoplethysmography and its application in clinical physiological measurement. *Physiological Measurement* **28**, 1–39 (2007). <https://doi.org/10.1088/0967-3334/28/3/R01>
- [3] Tamura, T.: Current progress of photoplethysmography and spo2 for health monitoring. *Biomedical Engineering Letters* **9** (2019). <https://doi.org/10.1007/s13534-019-00097-w>
- [4] Fonseca, P., Weysen, T., Goelema, M.S., Møst, E.I.S., Radha, M., Lunsingh Scheurleer, C., van den Heuvel, L., Aarts, R.M.: Validation of Photoplethysmography-Based Sleep Staging Compared With Polysomnography in Healthy Middle-Aged Adults. *Sleep* **40**(7) (2017). <https://doi.org/10.1093/sleep/zsx097>
- [5] Kinnunen, H., Rantanen, A., Kenttä, T., Koskimäki, H.: Feasible assessment of recovery and cardiovascular health: Accuracy of nocturnal hr and hrv assessed via ring ppg in comparison to medical grade ecg. *Physiological Measurement* **41** (2020). <https://doi.org/10.1088/1361-6579/ab840a>
- [6] Álvarez Casado, C., Paananen, P., Siirtola,

P., Pirttikangas, S., Bordallo López, M.: Meditation detection using sensors from wearable devices. In: Adjunct Proceedings of the International Joint Conference on Pervasive and Ubiquitous Computing, pp. 112–116. ACM, New York, NY, USA (2021). <https://doi.org/10.1145/3460418.3479318>

[7] Seshadri, D.R., Li, R.T., Voos, J.E., Rowbottom, J.R., Alfes, C.M., Zorman, C.A., Drummond, C.K.: Wearable sensors for monitoring the internal and external workload of the athlete. *NPJ Digital Medicine* **2** (2019)

[8] Sun, Y., Thakor, N.: Photoplethysmography revisited: From contact to noncontact, from point to imaging. *IEEE transactions on biomedical engineering* **63** (2015). <https://doi.org/10.1109/TBME.2015.2476337>

[9] Khanam, F.-T.-Z., Al-Naji, A., Chahl, J.: Remote monitoring of vital signs in diverse non-clinical and clinical scenarios using computer vision systems: A review. *Applied Sciences* **9**(20) (2019). <https://doi.org/10.3390/app9204474>

[10] Cheng, C.-H., Wong, K.-L., Chin, J.-W., Chan, T.-T., So, R.H.Y.: Deep learning methods for remote heart rate measurement: A review and future research agenda. *Sensors* **21**(18) (2021). <https://doi.org/10.3390/s21186296>

[11] Ni, A., Azarang, A., Kehtarnavaz, N.: A review of deep learning-based contactless heart rate measurement methods. *Sensors* **21**, 3719 (2021). <https://doi.org/10.3390/s21113719>

[12] Verkruysse, W., Svaasand, L.O., Nelson, J.S.: Remote plethysmographic imaging using ambient light. *Opt. Express* **16**(26), 21434–21445 (2008). <https://doi.org/10.1364/OE.16.021434>

[13] Poh, M.-Z., McDuff, D.J., Picard, R.W.: Advancements in noncontact, multiparameter physiological measurements using a web-cam. *IEEE Transactions on Biomedical Engineering* **58**(1), 7–11 (2011). <https://doi.org/10.1109/TBME.2010.2086456>

[14] Lewandowska, M., Rumiński, J., Kocejko, T., Nowak, J.: Measuring pulse rate with a web-cam — a non-contact method for evaluating cardiac activity. In: *Federated Conference on Computer Science and Information Systems (FedCSIS)*, pp. 405–410 (2011)

[15] de Haan, G., Jeanne, V.: Robust pulse rate from chrominance-based rppg. *IEEE Transactions on Biomedical Engineering* **60**(10), 2878–2886 (2013). <https://doi.org/10.1109/TBME.2013.2266196>

[16] Haan, G., Leest, A.: Improved motion robustness of remote-ppg by using the blood volume pulse signature. *Physiological measurement* **35**, 1913–1926 (2014). <https://doi.org/10.1088/0967-3334/35/9/1913>

[17] Li, X., Chen, J., Zhao, G., Pietikäinen, M.: Remote heart rate measurement from face videos under realistic situations. In: *2014 IEEE Conference on Computer Vision and Pattern Recognition*, pp. 4264–4271 (2014). <https://doi.org/10.1109/CVPR.2014.543>

[18] Wang, W., Stuijk, S., de Haan, G.: A novel algorithm for remote photoplethysmography: Spatial subspace rotation. *IEEE Transactions on Biomedical Engineering* **63**(9), 1974–1984 (2016). <https://doi.org/10.1109/TBME.2015.2508602>

[19] Yang, Y., Liu, C., Yu, H., Shao, D., Tsow, F., Tao, N.: Motion robust remote photoplethysmography in cielab color space. *Journal of Biomedical Optics* **21**, 117001 (2016). <https://doi.org/10.1117/1.JBO.21.11.117001>

[20] Wang, W., den Brinker, A.C., Stuijk, S., de Haan, G.: Algorithmic principles of remote ppg. *IEEE Transactions on Biomedical Engineering* **64**(7), 1479–1491 (2017). <https://doi.org/10.1109/TBME.2016.2609282>

[21] Pilz, C.S., Zaunseder, S., Krajewski, J., Blazek, V.: Local group invariance for heart rate estimation from face videos in the wild. In: *2018 IEEE/CVF Conference on Computer Vision and Pattern Recognition Workshops (CVPRW)*, pp. 1335–13358 (2018). <https://doi.org/10.1109/>

CVPRW.2018.00172

[22] Gudi, A., Bittner, M., van Gemert, J.: Real-time webcam heart-rate and variability estimation with clean ground truth for evaluation. *Applied Sciences* **10**(23) (2020). <https://doi.org/10.3390/app10238630>

[23] Spetlik, R., Franc, V., Cech, J., Matas, J.: Visual heart rate estimation with convolutional neural network. In: *BMVC* (2018)

[24] Chen, W.V., McDuff, D.J.: Deepphys: Video-based physiological measurement using convolutional attention networks. *ArXiv abs/1805.07888* (2018)

[25] Niu, X., Han, H., Shan, S., Chen, X.: Rhythmnet: End-to-end heart rate estimation from face via spatial-temporal representation. *CoRR abs/1910.11515* (2019) <https://arxiv.org/abs/1910.11515>

[26] Yu, Z., Peng, W., Li, X., Hong, X., Zhao, G.: Remote heart rate measurement from highly compressed facial videos: An end-to-end deep learning solution with video enhancement. In: *IEEE/CVF International Conference on Computer Vision (ICCV)*, pp. 151–160 (2019). <https://doi.org/10.1109/ICCV.2019.00024>

[27] Yu, Z., Li, X., Niu, X., Shi, J., Zhao, G.: Autohr: A strong end-to-end baseline for remote heart rate measurement with neural searching. *CoRR abs/2004.12292* (2020) <https://arxiv.org/abs/2004.12292>

[28] Lee, E., Chen, E., Lee, C.-Y.: Meta-rppg: Remote heart rate estimation using a transductive meta-learner. In: Vedaldi, A., Bischof, H., Brox, T., Frahm, J.-M. (eds.) *Computer Vision – ECCV 2020*, pp. 392–409. Springer, Cham (2020)

[29] Song, R., Chen, H., Cheng, J., Li, C., Liu, Y., Chen, X.: Pulsegan: Learning to generate realistic pulse waveforms in remote photoplethysmography. *IEEE Journal of Biomedical and Health Informatics* **PP**, 1–1 (2021). <https://doi.org/10.1109/JBHI.2021.3051176>

[30] Cheng, C.-H., Wong, K.-L., Chin, J.-W., Chan, T.-T., So, R.H.Y.: Deep learning methods for remote heart rate measurement: A review and future research agenda. *Sensors* **21**(18) (2021). <https://doi.org/10.3390/s21186296>

[31] Zhan, Q., Wang, W., de Haan, G.: Analysis of cnn-based remote-ppg to understand limitations and sensitivities. *Biomed. Opt. Express* **11**(3), 1268–1283 (2020). <https://doi.org/10.1364/BOE.382637>

[32] Boccignone, G., Conte, D., Cuculo, V., D’Amelio, A., Grossi, G., Lanzarotti, R.: An open framework for remote-ppg methods and their assessment. *IEEE Access* **8**, 216083–216103 (2020). <https://doi.org/10.1109/ACCESS.2020.3040936>

[33] Zhang, K., Zhang, Z., Li, Z., Qiao, Y.: Joint face detection and alignment using multitask cascaded convolutional networks. *IEEE Signal Processing Letters* **23**(10), 1499–1503 (2016). <https://doi.org/10.1109/lsp.2016.2603342>

[34] Felzenszwalb, P.F., Girshick, R.B., McAllester, D., Ramanan, D.: Object detection with discriminatively trained part-based models. *IEEE Transactions on Pattern Analysis and Machine Intelligence* **32**(9), 1627–1645 (2010). <https://doi.org/10.1109/TPAMI.2009.167>

[35] King, D.E.: Dlib-ml: A machine learning toolkit. *Journal of Machine Learning Research* **10**, 1755–1758 (2009)

[36] Liu, W., Anguelov, D., Erhan, D., Szegedy, C., Reed, S.E., Fu, C., Berg, A.C.: SSD: single shot multibox detector. *CoRR abs/1512.02325* (2015) <https://arxiv.org/abs/1512.02325>

[37] Sanchez-Moreno, A.S., Olivares-Mercado, J., Hernandez-Suarez, A., Toscano-Medina, K., Sanchez-Perez, G., Benitez-Garcia, G.: Efficient face recognition system for operating in unconstrained environments. *Journal of Imaging* **7**(9) (2021). <https://doi.org/10.3390/jimaging7090161>

[38] Kazemi, V., Sullivan, J.: One millisecond face alignment with an ensemble of regression trees. In: 2014 IEEE Conference on Computer Vision and Pattern Recognition, pp. 1867–1874 (2014). <https://doi.org/10.1109/CVPR.2014.241>

[39] Kowalski, M., Naruniec, J., Trzcinski, T.: Deep alignment network: A convolutional neural network for robust face alignment. CoRR **abs/1706.01789** (2017) <https://arxiv.org/abs/1706.01789>

[40] Álvarez Casado, C., Bordallo López, M.: Real-time face alignment: evaluation methods, training strategies and implementation optimization. Journal of Real-Time Image Processing, 1–29 (2021)

[41] Gross, R., Matthews, I., Cohn, J., Kanade, T., Baker, S.: Multi-pie. Image Vision Comput. **28**(5), 807–813 (2010). <https://doi.org/10.1016/j.imavis.2009.08.002>

[42] Rakshit, H., Ullah, M.A.: A comparative study on window functions for designing efficient fir filter. In: 2014 9th International Forum on Strategic Technology (IFOST), pp. 91–96 (2014). <https://doi.org/10.1109/IFOST.2014.6991079>

[43] Unakafov, A.M.: Pulse rate estimation using imaging photoplethysmography: generic framework and comparison of methods on a publicly available dataset. Biomedical Physics & Engineering Express **4**(4), 045001 (2018). <https://doi.org/10.1088/2057-1976/aabd09>

[44] Ly, B., Dyer, E., Feig, J., Chien, A., Bino, S.: Research techniques made simple: Cutaneous colorimetry: A reliable technique for objective skin color measurement. The Journal of investigative dermatology **140**, 3–121 (2020). <https://doi.org/10.1016/j.jid.2019.11.003>

[45] Teng, X.-F., Zhang, Y.-T.: Theoretical study on the effect of sensor contact force on pulse transit time. IEEE Transactions on Biomedical Engineering **54**(8), 1490–1498 (2007). <https://doi.org/10.1109/TBME.2007.900815>

[46] Liu, H., Allen, J., Khalid, S.G., Chen, F., Zheng, D.: Filtering-induced time shifts in photoplethysmography pulse features measured at different body sites: the importance of filter definition and standardization. Physiological Measurement **42**(7), 074001 (2021). <https://doi.org/10.1088/1361-6579/ac0a34>

[47] Fine, J., Branan, K.L., Rodriguez, A.J., Boonya-ananta, T., Ajmal, Ramella-Roman, J.C., McShane, M.J., Côté, G.L.: Sources of inaccuracy in photoplethysmography for continuous cardiovascular monitoring. Biosensors **11**(4) (2021). <https://doi.org/10.3390/bios11040126>

[48] Hartmann, V., Liu, H., Chen, F., Hong, W., Hughes, S., Zheng, D.: Toward accurate extraction of respiratory frequency from the photoplethysmogram: Effect of measurement site. Frontiers in Physiology **10**, 732 (2019). <https://doi.org/10.3389/fphys.2019.00732>

[49] Rodríguez, A., Ramos, J.: Video pulse rate variability analysis in stationary and motion conditions. Biomedical engineering online **17**, 11 (2018). <https://doi.org/10.1186/s12938-018-0437-0>

[50] Francis, J.G.F.: The QR Transformation—Part 2. The Computer Journal **4**(4), 332–345 (1962). <https://doi.org/10.1093/comjnl/4.4.332>

[51] Householder, A.S.: Unitary triangularization of a nonsymmetric matrix. J. ACM **5**(4), 339–342 (1958). <https://doi.org/10.1145/320941.320947>

[52] Sharma, A., Paliwal, K., Imoto, S., Miyano, S.: Principal component analysis using qr decomposition. International Journal of Machine Learning and Cybernetics **4** (2013). <https://doi.org/10.1007/s13042-012-0131-7>

[53] Eke, A., Herman, P., Kocsis, L., Kozák, L.: Fractal characterization of complexity in physiological temporal signals. Physiol Meas **23**, 31–38 (2002)

[54] Goldberger, A.L., Amaral, L.A.N., Glass, L., Hausdorff, J.M., Ivanov, P.C., Mark,

R.G., Mietus, J.E., Moody, G.B., Peng, C.-K., Stanley, H.E.: Physiobank, physiotoolkit, and physionet. *Circulation* **101**(23), 215–220 (2000). <https://doi.org/10.1161/01.CIR.101.23.e215>

[55] Katz, M.J.: Fractals and the analysis of waveforms. *Computers in biology and medicine* **18**(3), 145–156 (1988)

[56] Peng, C.-K., Havlin, S., Stanley, H., Goldberger, A.: Quantification of scaling exponents and crossover phenomena in nonstationary heartbeat time series. *Chaos: An Interdisciplinary Journal of Nonlinear Science* **5**, 82 (1995)

[57] Stricker, R., Müller, S., Gross, H.-M.: Non-contact video-based pulse rate measurement on a mobile service robot. In: The 23rd IEEE International Symposium on Robot and Human Interactive Communication, pp. 1056–1062 (2014). <https://doi.org/10.1109/ROMAN.2014.6926392>

[58] Heusch, G., Anjos, A., Marcel, S.: A reproducible study on remote heart rate measurement. *CoRR* **abs/1709.00962** (2017) <https://arxiv.org/abs/1709.00962>

[59] Bobbia, S., Macwan, R., Benezeth, Y., Mansouri, A., Dubois, J.: Unsupervised skin tissue segmentation for remote photoplethysmography. *Pattern Recognition Letters* **124**, 82–90 (2019). <https://doi.org/10.1016/j.patrec.2017.10.017>

[60] Soleymani, M., Lichtenauer, J., Pun, T., Pantic, M.: A multimodal database for affect recognition and implicit tagging. *IEEE Transactions on Affective Computing* **3**(1), 42–55 (2012). <https://doi.org/10.1109/T-AFFC.2011.25>

[61] Rapczynski, M., Werner, P., Al-Hamadi, A.: Effects of video encoding on camera based heart rate estimation. *IEEE Transactions on Biomedical Engineering* **PP**, 1–1 (2019). <https://doi.org/10.1109/TBME.2019.2904326>

[62] Lin, Y., Lin, Y.-H.: A study of color illumination effect on the snr of rppg signals, vol. 2017, pp. 4301–4304 (2017). <https://doi.org/10.1109/EMBC.2017.8037807>